



**HAL**  
open science

# Curious Binding Energy Increase between the Receptor-Binding Domain of the SARS-CoV-2 Spike Protein and Angiotensin-Converting Enzyme 2 Adsorbed on a Silane Monolayer from Molecular Dynamics Simulations

Solene Lecot, Yann Chevolut, Magali Phaner-Goutorbe, Christelle Yeromonahos

## ► To cite this version:

Solene Lecot, Yann Chevolut, Magali Phaner-Goutorbe, Christelle Yeromonahos. Curious Binding Energy Increase between the Receptor-Binding Domain of the SARS-CoV-2 Spike Protein and Angiotensin-Converting Enzyme 2 Adsorbed on a Silane Monolayer from Molecular Dynamics Simulations. *Journal of Physical Chemistry B*, 2021, 125 (39), pp.11078-11090. 10.1021/acs.jpcc.1c06050 . hal-03622153

**HAL Id: hal-03622153**

**<https://hal.science/hal-03622153>**

Submitted on 5 Apr 2022

**HAL** is a multi-disciplinary open access archive for the deposit and dissemination of scientific research documents, whether they are published or not. The documents may come from teaching and research institutions in France or abroad, or from public or private research centers.

L'archive ouverte pluridisciplinaire **HAL**, est destinée au dépôt et à la diffusion de documents scientifiques de niveau recherche, publiés ou non, émanant des établissements d'enseignement et de recherche français ou étrangers, des laboratoires publics ou privés.

This document is confidential and is proprietary to the American Chemical Society and its authors. Do not copy or disclose without written permission. If you have received this item in error, notify the sender and delete all copies.

**The Curious Binding Energy Increase between the Receptor-Binding Domain of the SARS-CoV-2 Spike Protein and the Angiotensin-Converting Enzyme 2 Adsorbed on a Silane Monolayer, from Molecular Dynamics Simulations.**

Journal:	<i>The Journal of Physical Chemistry</i>
Manuscript ID	jp-2021-060506.R1
Manuscript Type:	Article
Date Submitted by the Author:	n/a
Complete List of Authors:	Lecot, Solène; Ecole Centrale de Lyon Chevolot, Yann; CNRS, Phaner-Goutorbe, Magali; Ecole Centrale de Lyon, Yeromonahos, Christelle; Ecole Centrale de Lyon,

SCHOLARONE™  
Manuscripts

1  
2  
3  
4 The Curious Binding Energy Increase between the  
5  
6  
7  
8 Receptor-Binding Domain of the SARS-CoV-2  
9  
10  
11  
12 Spike Protein and the Angiotensin-Converting  
13  
14  
15  
16 Enzyme 2 Adsorbed on a Silane Monolayer, from  
17  
18  
19  
20  
21 Molecular Dynamics Simulations.  
22  
23  
24  
25  
26  
27  
28  
29

30 *Solène Lecot<sup>§</sup>, Yann Chevolut<sup>§§</sup>, Magali Phaner-Goutorbe<sup>§</sup>, Christelle Yeromonahos<sup>§\*</sup>*  
31  
32  
33  
34

35 <sup>§</sup> Université de Lyon, Ecole Centrale de Lyon, CNRS, INSA Lyon, Université Claude  
36  
37 Bernard Lyon 1, CPE Lyon, INL, UMR5270, 69130 Ecully, France  
38  
39

40 <sup>§</sup> Université de Lyon, CNRS, Ecole Centrale de Lyon, INSA Lyon, Université Claude Bernard  
41  
42 Lyon 1, CPE Lyon, CNRS, INL, UMR5270, 69130 Ecully, France  
43  
44  
45  
46  
47  
48  
49  
50

51 \* Corresponding Author  
52  
53

54 Christelle Yeromonahos: christelle.yeromonahos@ec-lyon.fr, + 33 4 72 18 62 35  
55  
56  
57  
58  
59  
60

**Abstract**

In the context of the Covid-19 outbreak since December 2019, antigenic tests are widely used, for diagnosis purpose, to detect the SARS-CoV-2 spike protein in nasopharyngeal fluid through its interactions with specific antibodies. However, the SARS-CoV-2 spike protein is subject to rapid mutations yielding more and more variants which might lose their affinity towards the currently used antibodies. The virus entry into the host cell involves interactions between the Angiotensin-Converting Enzyme 2 and the SARS-CoV-2 spike protein receptor binding domain, which should be preserved whatever the mutations to keep the infectious potential of the virus. However, as the enzyme has not evolved to recognize the virus, its affinity with the spike protein receptor binding domain is lower than with the specific antibodies. The present molecular dynamics simulations study suggests that the adsorption of the Angiotensin-Converting Enzyme 2 on specific silane monolayers could increase its affinity towards the spike protein receptor binding domain. Indeed silane monolayer, combining silane molecules with short alkyl chains and positively charged head-groups and silane molecules without charged head-groups, could adsorb the Angiotensin-Converting Enzyme 2 while keeping its bioactivity (orientation compatible with the spike protein trapping, low conformational changes) and increasing its interactions with the spike protein receptor binding domain (number of hydrogen bonds and electrostatic interactions) to lead to an increase by 20% both in the binding free energy and in the enzyme / receptor binding domain rupture force. This work could help to develop biosensing tools efficient towards any variants of the SARS-CoV-2 spike protein.

## Introduction

Antigenic tests are widely used as diagnosis tools in the context of the Covid-19 outbreak since December 2019. These tests, based on the molecular recognition of the SARS-CoV-2 spike protein RBD (S-RBD) by specific highly potent antibodies, yield rapid, sensitive, and specific diagnosis. However, the SARS-CoV-2 spike protein is currently subject to many mutations. Once mutated, the variants could lose their affinity towards the identified antibodies. However, the affinity between any variants of the SARS-CoV-2 spike protein RBD and the Angiotensin-Converting Enzyme 2 (ACE2) should be preserved. Indeed, the entry of the virus into the host cell involves interactions between ACE2 and S-RBD.<sup>1-4</sup> Consequently, ACE2 could be a target with limited mutation escaping possibilities. Some study report on the development of tools for the detection of the SARS-CoV-2 spike protein through its interactions with ACE2 in solution or on paper.<sup>5</sup> Nevertheless, as ACE2 has not evolved to recognize the spike protein, the affinity between ACE2 and S-RBD needs to be improved for clinical diagnosis use.<sup>6</sup>

Several studies have investigated the interactions between ACE2 and the SARS-CoV-2 spike protein both to better understand the infection process,<sup>7-11</sup> and to develop therapeutic approaches.<sup>6, 12-14</sup> In particular, the crystal structure of ACE2 cellular receptor in complex with S-RBD has been resolved.<sup>15,16</sup> Wang et al. have identified 21 residues from S-RBD and 16 hydrogen bonds at the binding interface with ACE2,<sup>16</sup> while Lan et al. have reported 17 residues from S-RBD in contact with 20 residues of ACE2, allowing the formation of 13 hydrogen bonds and 2 salt bridges at the interface.<sup>15</sup> Also, by using a molecular docking approach, Chen et al. have reported a stronger affinity between ACE2 and S- RBD than between ACE2 and the SARS-CoV-1 spike protein RBD, and identified a strong interaction between the residue F486 from S-RBD and the ACE2 hydrophobic pocket including the residues F28, L79, Y83 and L97.<sup>8</sup> Likewise, He et al. have determined by Molecular Mechanics Poisson-Boltzmann Surface Area (MMPBSA) the binding free energy between ACE2 and S-RBD.<sup>10</sup> The complex ACE2 – S-

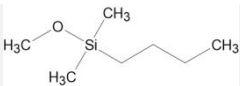
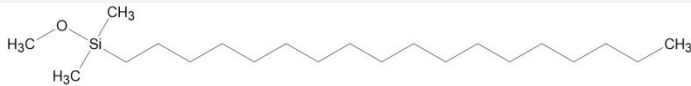
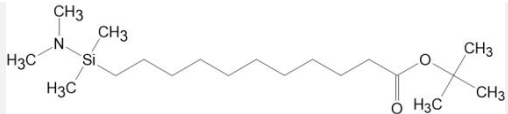
1  
2  
3 RBD was found significantly more stable than the complex ACE2 – SARS-CoV-1 spike protein  
4  
5 RBD. Moreover, Chan et al. have suggested thanks to deep mutagenesis and flow cytometry  
6  
7 experiments that mutations in the asparagine 90-glycosylation motif of ACE2 could increase  
8  
9 the affinity between ACE2 and S-RBD. Such ACE2 variant could be used to develop decoy  
10  
11 receptors with high affinity.<sup>6</sup> From a therapeutic point of view, Yang et al. have combined  
12  
13 Atomic Force Microscopy (AFM) experiments and Molecular Dynamics (MD) simulations, to  
14  
15 investigate the inhibitor effect of ACE2-derived peptides to reduce the complex formation  
16  
17 between ACE2 and S-RBD.<sup>3</sup>  
18  
19  
20  
21

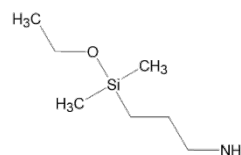
22 Protein adsorption is used in analytical devices as a simple immobilization mean to trap analytes  
23  
24 to be detected through protein / analyte interactions. However, the orientation and  
25  
26 conformation of the adsorbed proteins need to be controlled to preserve their ability to trap the  
27  
28 targeted analyte. Among surfaces, silane monolayers are commercially available and widely  
29  
30 used to immobilize proteins for biosensing purposes. However, it has been demonstrated that  
31  
32 the nature of the silane monolayer influences the protein activity and trapping efficiency.<sup>17,18</sup>  
33  
34 For example, among three different aminated silane molecules, the ones terminated by Chitosan  
35  
36 head-groups could allow the highest antigen-antibody binding capacity.<sup>17</sup> Indeed, silane  
37  
38 monolayers are expected to induce conformational changes in the adsorbed proteins which  
39  
40 could lead to a weakening or a strengthening of protein – analytes interactions.<sup>19</sup> MD  
41  
42 simulations are well-adapted to investigate the conformation and orientation of protein  
43  
44 adsorbed on surfaces, protein – surface interactions and protein – protein interactions at atomic  
45  
46 scale. In a previous MD simulation study, we have investigated the adsorption of streptavidin  
47  
48 on silane monolayers and the impact of streptavidin adsorption-induced conformational  
49  
50 changes on its interactions with biotin. From the calculation of the streptavidin – biotin rupture  
51  
52 force by steered molecular dynamic simulations (SMD), we have shown that silane molecules  
53  
54 with charged head-groups, as well as silane molecules with long alkyl chains, induce  
55  
56  
57  
58  
59  
60

conformational changes on streptavidin residues close to the biotin binding pocket which weaken streptavidin – biotin interactions. On the contrary, highly hydrophobic silane molecules with short alkyl chains and with neutral head-groups would lead to the lowest adsorption-induced conformational changes in streptavidin, and to a streptavidin-biotin rupture force similar to that obtained, from SMD simulations and AFM experiments,<sup>20</sup> in the native state of the complex (*i.e.*, in water without silane monolayer).<sup>19</sup>

In this work, we investigate by MD simulations, the effects of different silane monolayers on the adsorption of ACE2 (orientation of adsorbed ACE2, global and local adsorption-induced conformational changes), and the resulting effects on the affinity between ACE2 and S-RBD (conformational change in the residues at the interface between ACE2 and S-RBD, free binding energy and rupture force between adsorbed ACE2 and S-RBD). The six different silane monolayers investigated are elaborated from 3-aminopropyldimethylethoxysilane (C<sub>7</sub>H<sub>19</sub>NOSi named NH<sub>3</sub><sup>+</sup>), butyldimethylmethoxysilane (C<sub>7</sub>H<sub>18</sub>OSi named CH<sub>3</sub> short), octadecyldimethylmethoxysilane (C<sub>21</sub>H<sub>46</sub>OSi named CH<sub>3</sub> long), and tert-butyl-11-(dimethylamino(dimethyl)silyl)undecanoate (C<sub>19</sub>H<sub>41</sub>NO<sub>2</sub>Si, leading to COO<sup>-</sup> after deprotection), a mix (1:1) of CH<sub>3</sub> short and NH<sub>3</sub><sup>+</sup> silane molecules (named mix short), and a mix (1:1) of CH<sub>3</sub> long and NH<sub>3</sub><sup>+</sup> silane molecules (named mix long) (Table 1).<sup>19</sup>

**Table 1.** Composition of the six silane monolayers.

Silane monolayer	Silane molecule	Silane structure
CH <sub>3</sub> short	butyldimethylmethoxysilane	
CH <sub>3</sub> long	octadecyl-dimethylmethoxysilane	
COO <sup>-</sup>	(dimethylamino)-dimethylsilylundecanoate	

$\text{NH}_3^+$ 3-aminopropyl-  
dimethylethoxy-silane**Mix short**Mix CH<sub>3</sub> short: NH<sub>3</sub><sup>+</sup> (1:1)**Mix long**Mix CH<sub>3</sub> long: NH<sub>3</sub><sup>+</sup> (1:1)

## Methods

This work is divided into three parts. Firstly, MD simulations of ACE2 on different types of silane monolayers were performed to select the monolayers that could lead to ACE2 adsorption with an orientation compatible with S-RBD trapping. Also, the adsorption-induced conformational changes in ACE2 were characterized. Secondly, three selected silane monolayers and the complex ACE2 – S-RBD were considered. Adsorption-induced conformational changes in ACE2 were characterized, especially at the interface with S-RBD and compared to the structure of the complex in water without surface. Finally, SMD simulations and Molecular Mechanics Poisson-Boltzmann Surface Area (MMPBSA) analysis gave insight into the impact of conformational changes on the strength of interactions between ACE2 and the S- RBD.

### *System description*

MD simulations were performed from the PDB crystal structure 6M0J of the ACE2 – S-RBD complex.<sup>15</sup> Water molecules were kept while the zinc and chloride ions were not considered. Regarding the surface, the amorphous SiO<sub>2</sub> layer was taken from Roscioni et al.<sup>21</sup> and resized to the simulation box dimensions with a 2nm-thickness by a home-made Python code. Silane monolayers were built following our process adapted from the method proposed by Roscioni et al.<sup>21</sup>, as we have previously described.<sup>19, 22, 23</sup> Shortly, hydrolyzed silane molecules were initially randomly positioned on the silica (SiO<sub>2</sub>) surface without using explicit bonding, allowing their spontaneous lateral organization. Six different silane monolayers were designed, all with a

1  
2  
3 surface coverage of  $3.0 \text{ nm}^{-2}$ . Four silane monolayers were built with the following silane  
4 molecules: 3-aminopropyltrimethoxysilane (APTES, named  $\text{NH}_3^+$ ), *n*-  
5 butyldimethylmethoxysilane (named  $\text{CH}_3$  short), octadecyldimethylmethoxysilane (named  
6  $\text{CH}_3$  long), and (dimethylamino)dimethylsilylundecanoate (named  $\text{COO}^-$ ). Furthermore, two  
7 silane monolayers were prepared by mixing two different types of silane molecules: the mix  
8 short monolayer was a combination (1:1) of  $\text{CH}_3$  short and  $\text{NH}_3^+$  silane molecules while the  
9 mix long monolayer was a combination (1:1) of  $\text{CH}_3$  long and  $\text{NH}_3^+$  silane molecules.<sup>19</sup> The  
10 structures of the obtained silane monolayers were validated in our previous study<sup>23</sup> by  
11 comparing several physical parameters (alkyl chain tilt angle, nematic order parameter, gauche  
12 defects, and the radial distribution functions of silane molecules) to experimental data and also  
13 to MD simulations data obtained with other types of silane molecules. Water molecules were  
14 added, as well as  $\text{Na}^+$  and  $\text{Cl}^-$  ions to compensate charges and at a concentration of 150 mM to  
15 reproduce physiological conditions. Eventually, a Lennard-Jones (LJ) wall was added at the top  
16 of the simulation box to avoid interactions between water molecules and the bottom side of the  
17  $\text{SiO}_2$  surface.

### 38 *Simulations details*

39  
40  
41 Simulations were achieved with the Gromacs software, version 5.1.3<sup>24</sup> and visualization was  
42 performed with VMD, version 1.9.3.<sup>25</sup> Energy minimization was done with the steepest descent  
43 method and the NVT and NPT equilibrations were performed for 100 ps each. Then, several  
44 production simulations were performed. The leap-frog algorithm was used for the integration  
45 of motion equations, with a time step of 2 fs. Constraints to bond parameters were applied with  
46 a LINCS algorithm. Temperature was kept at 300 K with a Nose-Hoover thermostat using a  
47 time constant of 0.4 ps, while pressure was maintained at 1 bar using a Parrinello-Rahman  
48 barostat and a time constant of 12 ps. The OPLS all-atom force-field<sup>26</sup> was used to describe  
49 ACE2 and S-RBD. The amorphous  $\text{SiO}_2$  layer and silane molecules were described with a  
50  
51  
52  
53  
54  
55  
56  
57  
58  
59  
60

force-field adapted from previous studies<sup>21,27</sup> and from the OPLS all-atom force-field,<sup>28</sup> as we have previously reported.<sup>19,23</sup> The OPLS all-atom force-field was also used to describe TIP4P water,<sup>29</sup> Na<sup>+</sup> ions<sup>30</sup> and Cl<sup>-</sup> ions,<sup>31</sup> while parameters for the LJ wall were taken from a recent study.<sup>32</sup> Long-range electrostatic interactions were calculated with the Particle Mesh Ewald method and a cut-off of 1 nm. A cut-off distance of 1 nm was also used for LJ potentials.

**Adsorption of ACE2 on six different silane monolayers.** ACE2 adsorption process on the six different silane monolayers was investigated by defining 25 simulation systems. The first system, used as a reference, was ACE2 in water without silane monolayer. The 24 other systems contained an amorphous SiO<sub>2</sub> surface functionalized with one of the 6 silane monolayers (NH<sub>3</sub><sup>+</sup>, CH<sub>3</sub> short, CH<sub>3</sub> long, COO<sup>-</sup>, mix short and mix long) and ACE2 initially set at 0.8 nm above the silane molecules with one of the four initial orientations defined in Figure 1. Initial orientations 2, 3 and 4 were obtained from the initial orientation 1, by a rotation of 180°, 90° and -90° along the *y* axis, respectively. Simulation box dimensions were 10.6 nm × 10.6 nm × 19 nm. 3 independent simulation replicas of 100 ns were performed for each system. So, 75 simulations of 100 ns were performed in total. Images of some of these systems at final state are given in Figure 2.

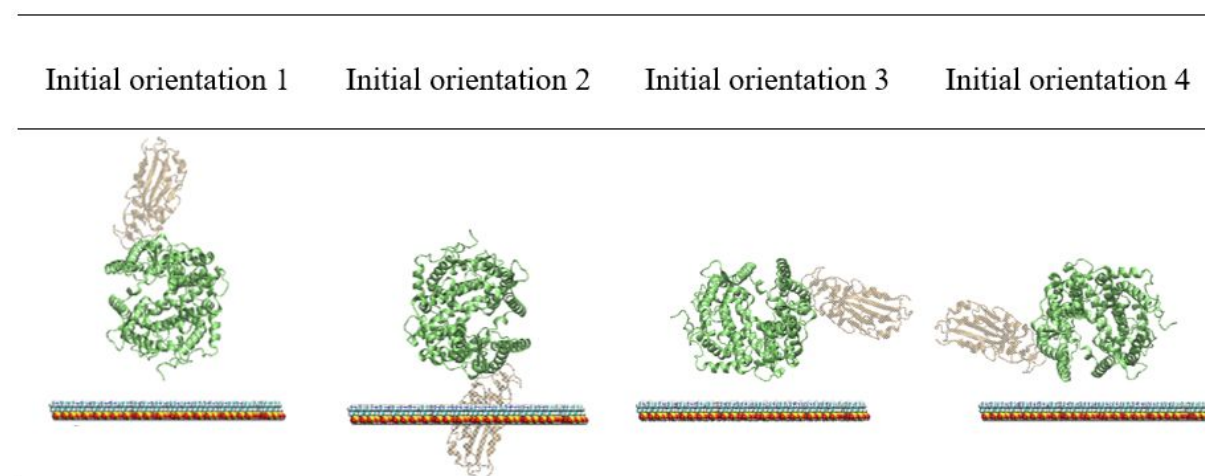


**Figure 1.** Illustration of the four initial orientations of the ACE2 cellular receptor above the mix short monolayer. The silane monolayer is 0.8 nm below ACE2. ACE2 is shown in green, atoms are shown in yellow (silicon), red (oxygen), cyan (carbon), white (hydrogen) and blue (nitrogen). For visualization purposes, the position of S-RBD is indicated in light brown.

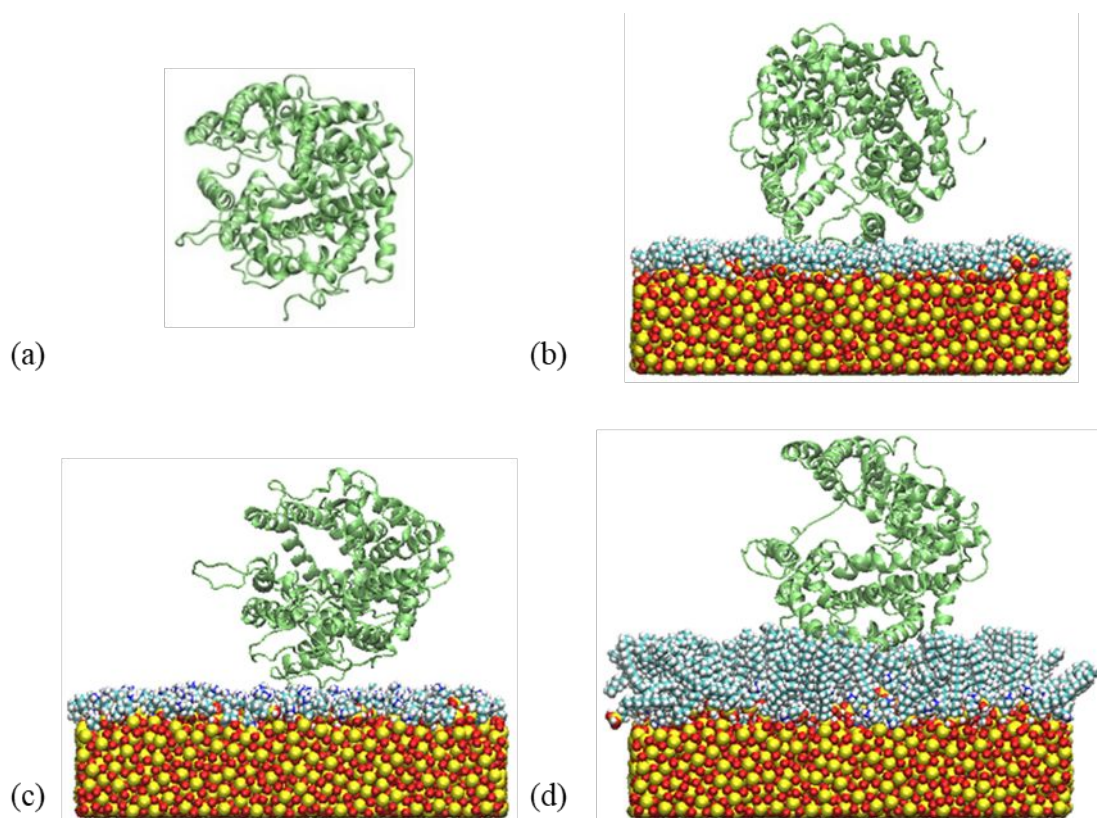
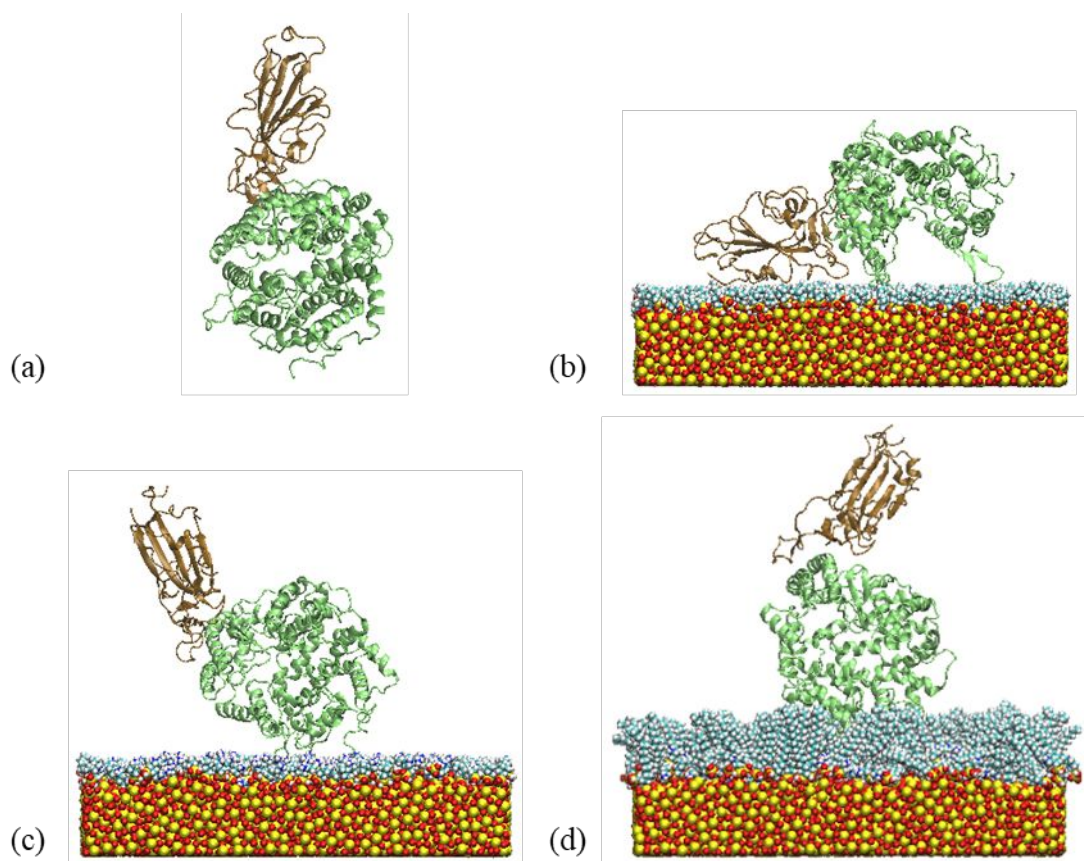


**Figure 2.** Representative images of four different systems at final state (after 100 ns MD simulations): ACE2 (a) in water, and adsorbed on silane monolayers (b)  $\text{CH}_3$  short (from the initial orientation 4), (c) mix short (from the initial orientation 1) and (d) mix long (from the initial orientation 1). ACE2 is shown in green. Atoms are shown in yellow (silicon), red (oxygen), cyan (carbon), white (hydrogen) and blue (nitrogen). The water molecules,  $\text{Na}^+$  and  $\text{Cl}^-$  ions, and the Lennard-Jones wall are not represented.

**Adsorption of the ACE2 - S-RBD complex on the selected silane monolayers.** The complex adsorption was investigated on the selected silane monolayers (*i.e.* the  $\text{CH}_3$  short, mix short, and mix long monolayers) and from the initial orientations identified at the first step. The

1  
2  
3 complex was initially positioned at 0.8 nm above the silane monolayers. Furthermore, another  
4 system was defined, including the complex in water without surface, which served as a  
5 reference. Simulation box dimensions were  $13.8 \times 13.8 \times 24$  nm. 6 independent simulation  
6 replicas of 200 ns were performed for each system. So, 24 simulations of 200 ns were performed  
7 in total. Representative images of the simulated systems at final state are given in Figure 3.  
8  
9  
10  
11  
12  
13  
14



44 **Figure 3.** Representative images of the four different systems at final state (after 200 ns MD  
45 simulations): ACE2– S-RBD complex (a) in water and adsorbed on silane monolayers (b)  
46 CH<sub>3</sub> short (from the initial orientation 4), (c) mix short (from the initial orientation 1) et (d)  
47 mix long (from the initial orientation 1). ACE2 is shown in green, while S-RBD is shown in  
48 brown, and atoms are shown in yellow (silicon), red (oxygen), cyan (carbon), white  
49 (hydrogen) and blue (nitrogen). The water molecules, Na<sup>+</sup> and Cl<sup>-</sup> ions and the Lennard-Jones  
50 wall are not represented.  
51  
52  
53  
54  
55  
56  
57  
58  
59  
60

1  
2  
3 **SMD simulations: S-RBD unbinding from ACE2.** Initial configurations of Steered Molecular  
4 Dynamics (SMD) simulations were selected among the final states of the 200-ns MD  
5 simulations modelling the complex in water and the complex adsorbed on the silane monolayers  
6 mix short and mix long. During SMD simulations, an external force was applied on the center-  
7 of-mass of S-RBD to pull it away from ACE2. Regarding the system with the complex in water,  
8 a position restriction was applied on the ACE2 center-of-mass to prevent its movement and to  
9 allow the detachment of S-RBD (the position restriction was applied on the ACE2 atom closest  
10 to its center of mass, excepting hydrogen atoms). On the contrary, no position restriction was  
11 applied on ACE2 for the systems where it was adsorbed on a silane monolayer, and no covalent  
12 bond was defined with the surface. Indeed, the Van der Waals and electrostatic interactions  
13 which were established between ACE2 and the SiO<sub>2</sub> layer functionalized with silane molecules  
14 were strong enough to prevent its desorption while S-RBD was pulled away by the applied  
15 force. This force was a harmonic potential, with a force constant  $k = 100$  pN/nm and a pulling  
16 velocity  $v = 2$  m.s<sup>-1</sup>. To reproduce AFM experiments, the force was applied on the spike protein  
17 in the direction normal to the surface. Two initial configurations were considered for each  
18 system. Simulation boxes were extended up to 32 nm to verify the minimum image convention.  
19 Energy minimization, NPT equilibration and simulation productions of 6 ns were performed.  
20 20 independent simulation replicas were achieved for each starting configuration.

#### 21 *Analysis parameters*

22  
23 The following parameters were investigated by using Gromacs analysis functions, g\_mmpbsa  
24 tools, VMD tools and home-made Python codes. Error bars correspond to the standard error of  
25 the values calculated for the different simulation replicas.

26  
27 The interaction energies between the silane monolayers and the ACE2 – S-RBD complex were  
28 investigated through the Van der Waals and electrostatic contributions. The ACE2 adsorption-  
29  
30

1  
2  
3 induced conformational changes were investigated by calculating the root-mean-square  
4 deviation (RMSD) and the root-mean-square fluctuation (RMSF), and the variations in the  
5 protein secondary structure. Also, the number of hydrogen bonds which are established between  
6 ACE2 and S-RBD were calculated. Finally, the contact surface between two elements is defined  
7 as following: atoms from ACE2 are considered in contact with the silane monolayer or with S-  
8 RBD if they are located at less than 0.4 nm from one atom of a silane molecule or of S-RBD,  
9 respectively. The given values are averaged over the last 10 ns of the MD simulations (100 ns  
10 or 200 ns).

11  
12  
13 **MMPBSA analysis.** Binding free energy between ACE2 and S-RBD ( $\Delta G$ ) is determined by  
14 MMPBSA with the `g_mmpbsa` tool.<sup>33</sup> Due to the approximations and hypothesis made during  
15 the calculation, MMPBSA results should not be interpreted quantitatively, but should be  
16 compared qualitatively between the different systems considered.<sup>34</sup> The given values are  
17 calculated over the last ns of the simulation (one point every 100 ps).

18  
19  
20 **SMD simulations.** The rupture force was calculated from the force - time curves and defined  
21 as the highest force applied on S-RBD before its detachment. Rupture force and detachment  
22 time were determined for each simulation replica. Mean values, standard deviation and  
23 histograms of the rupture force were calculated.

## 24 25 26 **Results and Discussion**

27  
28  
29 *Identification of the silane monolayers which are the most appropriate to adsorb the ACE2*  
30 *cellular receptor with an orientation compatible with the trapping of S-RBD.*

31  
32  
33 For biosensing purposes, we firstly deciphered if some silane monolayers could allow the  
34 systematic adsorption of ACE2, with an orientation compatible with the trapping of S-RBD.

1  
2  
3 Because of computational limitations, as simulations cannot be long enough to allow global  
4  
5  
6 reorientation of ACE2 around the silane monolayers before adsorption, four initial orientations  
7  
8  
9  
10 of ACE2 are studied, as shown Figure 1.

11  
12  
13  
14 Adsorption did barely influence the initial ACE2 orientations. The Van der Waals (VdW) and  
15  
16  
17 the electrostatic (elec) contributions to the interaction energy between ACE2 and the silane  
18  
19  
20 monolayers are calculated over three replicates, for each initial orientation. For each silane  
21  
22  
23 monolayer we defined the most likely trapping orientation as the one that leads both to a  
24  
25  
26 systematic adsorption of ACE2 (through all replicates) and to the most favorable interaction  
27  
28  
29 energy. Among the four orientations studied, orientation 1 is the best suited as the residues  
30  
31  
32 interacting with S-RBD are located on the top of the protein, exposed to the water bulk. On the  
33  
34  
35 contrary, ACE2 cannot interact with S-RBD with orientation 2, as interfacial residues are then  
36  
37  
38 located below the protein, in contact with the silane molecules. Orientations 3 and 4 seem to  
39  
40  
41 allow interactions with S-RBD but might be less favourable than orientation 1. Indeed, in the  
42  
43  
44 case of biosensing applications with several ACE2 adsorbed on the surface, orientations 3 and  
45  
46  
47 4 could lead to steric hindrances that might disturb S-RBD trapping. Evolution of the total VdW  
48  
49  
50 and elec interaction energy between ACE2 and the surface is shown in Supporting information,  
51  
52  
53 Figure S1, while immobilization frequencies (over three replicates) and interactions energies  
54  
55  
56 after ACE2 adsorption on silane monolayers are summarized in Supporting Information, Table  
57  
58  
59  
60 S1.

1  
2  
3 Regarding the CH<sub>3</sub> short monolayer, with orientation 1, results show that ACE2 is immobilized  
4 on the surface only for one of the three simulation replicates, and after 45 ns. With orientations  
5  
6 on the surface only for one of the three simulation replicates, and after 45 ns. With orientations  
7  
8 2, 3 and 4, the ACE2 cellular receptor is rapidly adsorbed on the surface for all simulation  
9  
10 replicas (less than 15 ns). The interaction energy is progressively stabilized, and initial  
11  
12 orientation 4 leads to the most favourable adsorption (*i.e.* to the lowest VdW and elec  
13  
14 interaction energies, about -122 kcal/mol). For NH<sub>3</sub><sup>+</sup> monolayer, ACE2 cellular receptor is  
15  
16 quickly and strongly adsorbed on the surface for all simulation replicas, regardless of its initial  
17  
18 orientation (interaction energy varies between -258 kcal/mol and -386 kcal/mol depending on  
19  
20 the initial orientation). However, the most likely orientation seems to be orientation 2 (-386  
21  
22 kcal/mol), which is not suitable for our application. Concerning the CH<sub>3</sub> long monolayer,  
23  
24 adsorption on silane monolayer for all simulation replicas is only observed with orientation 3.  
25  
26 However, the immobilization process is long, as interactions with the silane molecules appear  
27  
28 after more than 30 ns, 70 ns and 20 ns for each simulation replicas. In line with the long  
29  
30 adsorption process, the interaction energy between ACE2 and the CH<sub>3</sub> long monolayer is weak,  
31  
32 about -61 kcal/mol. Thus, the CH<sub>3</sub> long monolayer does not seem to be suitable for ACE2  
33  
34 adsorption. Regarding the COO<sup>-</sup> monolayer, few or no interaction appears between ACE2 and  
35  
36 the surface with ACE2 initial orientations 2, 3, and 4, while interactions appear after several  
37  
38 tens of ns in the case of orientation 1. However, a positive interaction energy between ACE2  
39  
40 and COO<sup>-</sup> silane molecules is obtained with orientation 1, showing that these interactions are  
41  
42 not favourable. This could be explained by the non-favourable electrostatic interactions  
43  
44 occurring between ACE2 (that is negatively charged -27 e) and the negative head-group charge  
45  
46 of the silane molecules. Concerning the mix short monolayer, ACE2 cellular receptor is rapidly  
47  
48 immobilized on the surface for all initial orientations (less than 5 ns, Supporting Information,  
49  
50 Figure S1). Furthermore, orientation 1 is the most likely regarding the interaction energy (about  
51  
52 -245 kcal/mol), while orientation 2 is the less likely (about -172 kcal/mol). Eventually, ACE2  
53  
54  
55  
56  
57  
58  
59  
60

1  
2  
3 cellular receptor is adsorbed on the mix long silane monolayer for all initial orientations and  
4 simulation replicas, orientation 1 being the most likely (about -256 kcal/mol) and orientation 2  
5 the less likely (about -201 kcal/mol). Thus, the mix short and the mix long silane monolayers  
6 seem well-suited to immobilize ACE2 with similar interaction energies (around -250 kcal/mol)  
7 with an orientation compatible with the trapping of S-RBD. Indeed, on these two monolayers  
8 the most probable ACE2 trapping orientation is the orientation 1. The CH<sub>3</sub> short silane  
9 monolayer could also be suitable for immobilizing ACE2, even if less favourable than the mix  
10 short and mix long monolayers. Indeed, the most likely ACE2 adsorption orientation is the  
11 orientation 4 (interaction energy around -122 kcal/mol), that could lead to a steric hindrance for  
12 S-RBD trapping if several ACE2 were adsorbed on the monolayer (Figure 2).

13  
14  
15  
16  
17  
18  
19  
20  
21  
22  
23  
24  
25  
26  
27 Conformational changes induced in ACE2 by its adsorption on the CH<sub>3</sub> short, mix short, and  
28 mix long silane monolayers are characterised by calculating the Root Mean Square Deviation  
29 (RMSD) of ACE2 (Supporting Information, Figure S2). RMSD values are  $3.2 \pm 0.3$  Å in water,  
30  $3.0 \pm 0.1$  Å when ACE2 is immobilized on CH<sub>3</sub> short monolayer,  $3.4 \pm 0.1$  Å on mix short  
31 monolayer and  $3.1 \pm 0.2$  Å on mix long monolayer (these values are calculated from the initial  
32 simulation step and the last 10 ns of the simulations, *i.e.* when the system is stabilized). RMSD  
33 values when ACE2 is adsorbed on silane monolayers are close to the one obtained in water.  
34 Thus, as for the streptavidin – biotin complex,<sup>19</sup> we suggest that the conformational changes  
35 induced by adsorption on silane monolayers are quite low, allowing to preserve the global  
36 structure of ACE2. Furthermore, Root Mean Square Fluctuations (RMSF) traces show that the  
37 mobility of ACE2 residues interacting with S-RBD is quite similar to the one observed in water  
38 (Supporting Information, Figure S3). Thus, it seems that the ability of ACE2 to interact with S-  
39 RBD could be preserved after its adsorption on the three identified silane monolayers.  
40  
41  
42  
43  
44  
45  
46  
47  
48  
49  
50  
51  
52  
53  
54  
55  
56  
57  
58 In the following, only the three identified silane monolayers (mix short, mix long, and CH<sub>3</sub>  
59 short) are studied.  
60

*Adsorption induced conformational changes in the ACE2 – S-RBD complex.*

**Interactions between the ACE2 – S-RBD complex and the CH<sub>3</sub> short, mix long and mix short silane monolayers.** It has been previously demonstrated that the adsorption and orientation of protein on charged surfaces is controlled by its electric dipole.<sup>35,36</sup> Thus, we have plotted the electric dipole moment<sup>37</sup> of the ACE2–S-RBD complex adsorbed on the mix short and mix long monolayers in Supporting Information, Figure S4. The dipole moment orientations are well coherent with the complex adsorption on a positively charged surface. Interactions between the complex and the silane monolayers CH<sub>3</sub> short, mix short and mix long were characterized by the interaction energy, the number of residues in the contact area between ACE2 and silane molecules and the type of ACE2 residues which are likely to interact with silane molecules (Table 2).

**Table 2.** Total VdW and elec interaction energy between the ACE2 – S-RBD complex and the silane monolayers, number of residues in the contact area between ACE2 and the silane monolayers, number of residues in the contact area between S-RBD and the silane monolayers, and list of ACE2 residues in contact with the silane monolayers.

System	CH <sub>3</sub> short	Mix short	Mix long
<b>Interaction energy complex – silanes (kcal/mol)</b>	-197.8 ± 31	-290.7 ± 25	-309.7 ± 24
<b>Number of residues in the contact area ACE2 – silane <sup>a</sup></b>	14.8 ± 2.3	15.5 ± 2.6	60.8 ± 5.5
<b>Number of residues in the contact area S-RBD – silane <sup>a</sup></b>	13.3 ± 4.1	0	0
<b>ACE2 residues in contact with the silane monolayer</b>	E56, E57, Q60, P135, D136, N137, P138, Q139, E140	D609, Y613, A614, D615	D136 to L142, L148, I151, N154, L156, D157, N159 to A164, E166, S167, S170, Y243, A246, K247, M249 to Y255, P258, I259, L281, V283, G286, Q287, V491 to D494, Q598 to F603, Y613 to D615

<sup>a</sup> A residue is considered in contact with the silane monolayer if one of its atoms is located at less than 0.4 nm from one atom of a silane molecule.

The interaction energy between the complex and silane molecules are lower with the mix long monolayer than with the mix short and CH<sub>3</sub> short silane monolayers while the contact area are higher. Indeed, with the mix long monolayer, numerous Van der Waals interactions are established between the long alkyl chains of CH<sub>3</sub> long silane molecules and ACE2 hydrophobic residues (A, L, P, V, I, M, F, W), in addition to electrostatic interactions between the NH<sub>3</sub><sup>+</sup> silane molecules and polar or negatively charged ACE2 residues (D, E).

Mix short silane monolayer shows a lower interaction energy and a lower contact surface with ACE2 than the CH<sub>3</sub> short silane monolayer. Indeed, electrostatic interactions are established between the positively charged NH<sub>3</sub><sup>+</sup> silane molecules of the mix short monolayer and ACE2 negatively charged residues (D609, D615). However, NH<sub>3</sub><sup>+</sup> silane molecules have also a repulsive impact on ACE2 positively charged residues, which could explain the lower contact surface. Furthermore, due to ACE2 orientation on the CH<sub>3</sub> short monolayer, some interactions are established between S-RBD and the silane molecules. Finally, the mix long and mix short monolayers seem to have the highest affinities with the studied complex. In the following, we characterize the structure of the complex adsorbed on the CH<sub>3</sub> short, mix short, and mix long monolayers.

**RMSD and secondary structure.** RMSD values of the ACE2 – S-RBD complex after ACE2 adsorption on the three studied silane monolayers are summarized in Table 3, while its secondary structure is characterized in Supporting Information, Table S2.

**Table 3.** RMSD values and number of hydrogen bonds between S-RBD and ACE2 for all systems studied.

System	RMSD <sub>complex</sub> (Å)	RMSD <sub>ACE2</sub> (Å)	RMSD <sub>S-RBD</sub> (Å)	Number of hydrogen bonds
In water	4.1 ± 0.2	3.9 ± 0.2	4.5 ± 0.4	9.1 ± 0.6
CH <sub>3</sub> short	4.2 ± 0.4	3.8 ± 0.2	5.3 ± 0.7	10.3 ± 0.7
Mix short	3.7 ± 0.2	3.5 ± 0.2	4.1 ± 0.2	11.9 ± 0.7
Mix long	4.2 ± 0.2	3.9 ± 0.2	4.8 ± 0.2	10.5 ± 0.6

1  
2  
3 The RMSD values of ACE2, of S-RBD, and of the complex in water are below 4.5 Å, in  
4 agreement with the value determined by Ali et al. from MD simulations.<sup>34</sup> So, the complex  
5 structure integrity, in water, is preserved through the simulation. Furthermore, the structure of  
6 the complex adsorbed on the studied silane monolayers seems well preserved, as its RMSD  
7 values are close to the one obtained in water. Also, the complex secondary structure is well-  
8 preserved after its adsorption on each studied silane monolayers (Table S2). So, these results  
9 suggest, once again, that the affinity between ACE2 adsorbed on the studied silane monolayers  
10 and S-RBD could be preserved.  
11  
12  
13  
14  
15  
16  
17  
18  
19  
20  
21

22 **RMSF.** To further characterize adsorption-induced conformational changes in the structure of  
23 the ACE2 – S-RBD complex, RMSF traces of the C<sub>α</sub> backbone of ACE2 and of S-RBD are  
24 given in Figure 4 for all systems, and summarized in Figure 5. In the case of the complex in  
25 water, the residues with high mobility are in accordance with the results from Ali et al.<sup>34</sup>  
26 Furthermore, the global evolution of RMSF traces is globally conserved when ACE2 is  
27 adsorbed on silane monolayers, in accordance with the above RMSD and secondary structure  
28 results. However, a few differences are observed for the ACE2 residues which are localized  
29 around the contact area with the silane monolayers, and around the interface with S-RBD.  
30  
31  
32  
33  
34  
35  
36  
37  
38  
39  
40  
41  
42  
43  
44  
45  
46  
47  
48  
49  
50  
51  
52  
53  
54  
55  
56  
57  
58  
59  
60

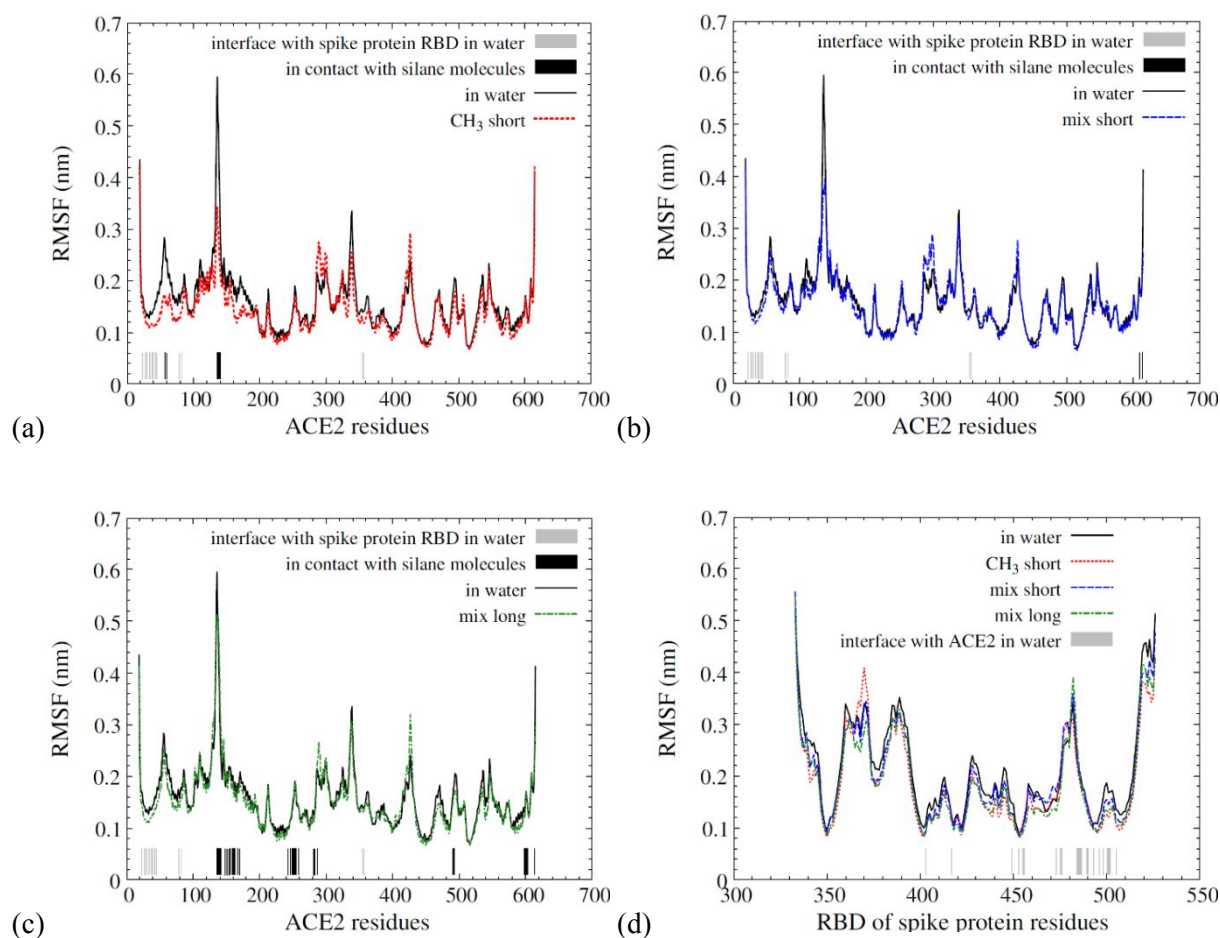


**Figure 4.** RMSF traces of the  $C_{\alpha}$  atoms of ACE2 adsorbed on silane monolayers (a)  $\text{CH}_3$  short, (b) mix short, and (c) mix long, and comparison with the one obtained in water, and (d) RMSF traces of the  $C_{\alpha}$  atoms of S-RBD for all systems. ACE2 residues interacting with S-RBD in water are indicated (grey lines), as well as ACE2 residues in contact with silane molecules (black lines).

Residue localization		Parameters (comparison with the reference system, i.e. the system in water without surface)	CH <sub>3</sub> short	Mix long	Mix short	Water without surface
S-RBD	In contact or close to the silane molecules	RMSF increase (Fig. 4)	367-372	-	-	reference
	Close to ACE2	RMSF increase (Fig. 4)	Around 472-476, around 484-505			reference
		Residues at the ACE2 – S-RBD interface	K417, Y449, Y453, L455, F456, Y473, A475, E484, G485, F486, N487, Y489, F490, Q493, G496, Q498*, T500*, N501, Y505			
			G446, L492, S494, G502	G446, G476, V483, L492, S494	G476, L492, F497, G502	R403*, G476, G502
		Stabilization of the interactions <sup>a</sup> (MMPBSA) (Fig. 6)	R403*, K417, K458, E484, F486, Y489, F490, Q493	R403*, F456, K458, V483, E484, G485, Q493	R403*, D405, E406, K417, L455, F456, K458, E484, F486, F490, Q493, Q498*, T500*	reference
Destabilization of the interactions <sup>a</sup> (MMPBSA) (Fig. 6)	T500*, N501, V503	N501	R408, Y449	reference		
ACE2	In contact or close to the silane molecules	RMSF decrease (Fig. 4)	60, 135-140	Around 615	135-140, around 615	reference
	Center of the protein	RMSF increase (Fig. 4)	280-300, 427			reference
	Close to S-RBD	RMSF decrease (Fig. 4)	24-40, 79-83, 353-357			reference
		Residues at the ACE2 – S-RBD interface	Q24, T27, F28, D30, K31*, H34, E35, E37*, D38*, Y41*, Q42, L45, L79, M82, Y83, K353*			
			I21, Q76, P84, G354	I21, Q76, R357	I21, G354, D355, R357, R393	G354, D355, R357
Stabilization of the interactions <sup>a</sup> (MMPBSA) (Fig. 6)		I21, E23, K31*, Q42, M82	E23, T27, M82	E23, L79, M82	reference	
Destabilization of the interactions <sup>a</sup> (MMPBSA) (Fig. 6)	S19, K26, K68, G354	E35, K353, G354	S19	reference		

**Figure 5.** ACE2 and S-RBD residues with a mobility different from that in water without surface. ACE2 residues in contact with S-RBD, and S-RBD residues in contact with ACE2. ACE2 and S-RBD residues with  $\Delta\Delta G \geq 0.4$  kcal/mol and  $\Delta\Delta G \leq 0.4$  kcal/mol. Residues identified as hot spots by Laurini et al.<sup>38</sup> are indicated by \*. <sup>a</sup> Residues with too large errors bars to have significant stabilizing or destabilizing effects are not indicated.

Most of the ACE2 residues in the contact areas with the different monolayers have either lower RMSF values than in water or the same values as in water. Indeed, in the case of the CH<sub>3</sub> short

1  
2  
3 silane monolayer, lower RMSF values are observed around the residues 60 and 135 to 140,  
4 which are in the contact area with silane molecules. Regarding the mix short monolayer, RMSF  
5 values are also lower around the residues 135 to 140, which are close to the silane molecules,  
6 as well as near the residue 615, which is in contact with silane molecules. Regarding the mix  
7 long silane monolayer, RMSF value is lower near the residue 615, which is in contact with the  
8 silane molecules. For the other ACE2 residues in contact with silane molecules, RMSF values  
9 are barely impacted by the interactions which are established with the silane molecules. On the  
10 contrary, for all silane monolayers, ACE2 RMSF traces show higher values near the residues  
11 280 to 300 and around the residue 427 than for the complex in water. These residues are close  
12 to the centre of ACE2. Regarding ACE2 residues which belong to the interface with S-RBD, a  
13 short decrease in the RMSF values is observed near the residues 24 to 45, 79 to 83, and 353 to  
14 357 for the three silane monolayers. However, the decrease is greater in the case of the CH<sub>3</sub>  
15 short monolayer, likely because of additional interactions between S-RBD and the monolayer.  
16  
17 Regarding S-RBD, RMSF traces are slightly modified when ACE2 is adsorbed on the silane  
18 monolayers, compared to the values obtained for the complex in water. Regarding the CH<sub>3</sub> short  
19 monolayer, a higher mobility is observed around the residues 367 to 372, which are in contact  
20 with some silane molecules in several simulation replicas. For all silane monolayers, some  
21 variations in the RMSF values are observed around the residues 472 to 476, and 484 to 505,  
22 which belong to the interface with ACE2. These results suggest that some small conformational  
23 changes appear in the complex when ACE2 is adsorbed on the CH<sub>3</sub> short, mix short and mix  
24 long silane monolayers, especially around the residues interacting with the silane molecules,  
25 but also for the residues located at the ACE2 / S-RBD interface. These changes are higher in  
26 the case of the CH<sub>3</sub> short monolayer than in the case of the mix short and mix long monolayers,  
27 likely because of the additional interactions between S-RBD and the CH<sub>3</sub> short molecules. This  
28  
29  
30  
31  
32  
33  
34  
35  
36  
37  
38  
39  
40  
41  
42  
43  
44  
45  
46  
47  
48  
49  
50  
51  
52  
53  
54  
55  
56  
57  
58  
59  
60

1  
2  
3 could induce some modifications in the nature of the residues belonging to the interface between  
4  
5 ACE2 and S-RBD.  
6  
7

8 **Interface between ACE2 and S-RBD.** The residues located at the interface between ACE2  
9  
10 and S-RBD are summarized in Figure 5 and defined as the ACE2 or S-RBD residues having  
11  
12 one atom located at less than 0.4 nm from an atom from the other protein.  
13  
14

15  
16 Results show that 19 ACE2 residues belong to the interface for the complex in water and when  
17  
18 it is adsorbed on the mix long silane monolayer, while 20 residues belong to the interface with  
19  
20 the CH<sub>3</sub> short monolayer, and 21 with the mix short monolayer. The five ACE2 residues  
21  
22 identified by Laurini et al as hot spots,<sup>38</sup> *i.e.*, the main interactions sites with S-RBD are D38,  
23  
24 K31, E37, K353 and Y41. These residues belong to the interface of all the studied systems, as  
25  
26 well as eleven additional residues Q24, T27, F28, D30, H34, E35, Q42, L45, L79, M82 and  
27  
28 Y83, in accordance with previous studies.<sup>15,16</sup> Furthermore, the residue I21 does not belong to  
29  
30 the interface for the complex in water, but it does with the three silane monolayers. Also, some  
31  
32 disparities appear depending on the type of silane monolayers. In particular, the residue R393  
33  
34 belongs to the interface in the case of the mix short monolayer, while for the mix long and CH<sub>3</sub>  
35  
36 short monolayers, the residue Q76 belongs to the interface, which is perturbed around the  
37  
38 residues G354 to R357, in accordance with the RMSF values.  
39  
40  
41  
42  
43  
44

45 Regarding S-RBD residues, 22 of them belong to the interface with ACE2 when the complex  
46  
47 is in water, while 23 residues belong to the interface when ACE2 is adsorbed on the CH<sub>3</sub> short  
48  
49 and mix short monolayer, and 24 with the mix long monolayer. Regarding the three hot-spot  
50  
51 residues identified by Laurini et al.,<sup>38</sup> Q498 and T500 residues are still located at the interface  
52  
53 with ACE2 when it is adsorbed on the silane monolayers, but not R403. These results are in  
54  
55 agreement with the RMSF calculations. A few other modifications are observed. Especially,  
56  
57 the L492 residue is added to the interface for all silane monolayers.  
58  
59  
60

These results suggest that the interface between ACE2 and S-RBD is impacted by ACE2 adsorption-induced conformational changes, which depend on the type of silane monolayer. This result could explain the increase in the number of hydrogen bonds between ACE2 and S-RBD observed when ACE2 is adsorbed on silane monolayers (Table 3). So, our results suggest that the interactions between ACE2 and S-RBD could be reinforced through ACE2 adsorption-induced conformational changes.

*Effect of silane monolayers on the binding free energy and rupture force between adsorbed ACE2 and S-RBD.*

**MMPBSA analysis.** Binding free energy between ACE2 and S-RBD were determined from MMPBSA calculations (Table 4) for the complex in water without surface and for ACE2 adsorbed on the CH<sub>3</sub> short, mix short and mix long monolayers. Due to the calculation method approximations, results are not interpreted quantitatively, but qualitatively compared between the different systems. Results show that the adsorption of ACE2 on silane monolayers lead to a decrease in the binding free energy, in comparison with the complex in water, suggesting a stabilization of the interactions between ACE2 and S-RBD. These results can be partly explained by the increase in the number of hydrogen bonds observed between ACE2 and S-RBD (Table 3).

**Table 4.** Binding free energy between ACE2 and S-RBD calculated by MMPBSA.

System	In water	CH <sub>3</sub> short	Mix short	Mix long
$\Delta G$ (kcal/mol)	$-63.0 \pm 2.6$	$-78.2 \pm 2.7$	$-74.7 \pm 3.7$	$-72.9 \pm 4.0$

To further understand the stabilization of the interactions between the adsorbed ACE2 and S-RBD, the contribution of each residue to the binding free energy was investigated. The binding energy change on each residue,  $i$ , is defined by analogy with the study of Laurini et al.<sup>38,39</sup>:

$$\Delta\Delta G^i = \Delta G^i_{\text{complex in water}} - \Delta G^i_{\text{complex adsorbed on silane monolayer}} \quad (1)$$

Thus, if  $\Delta\Delta G^i \geq 0$ , the residue contribution is stabilizing the ACE2 – S-RBD interactions, while if  $\Delta\Delta G \leq 0$ , the residue contribution shows a destabilizing effect. The residues with  $|\Delta\Delta G| \geq 0.4$  kcal/mol, *i.e.*, the main residues contributing to the stabilization or to the destabilization of the complex are shown in Figure 6 and summarized in Figure 5, for each different silane monolayers.

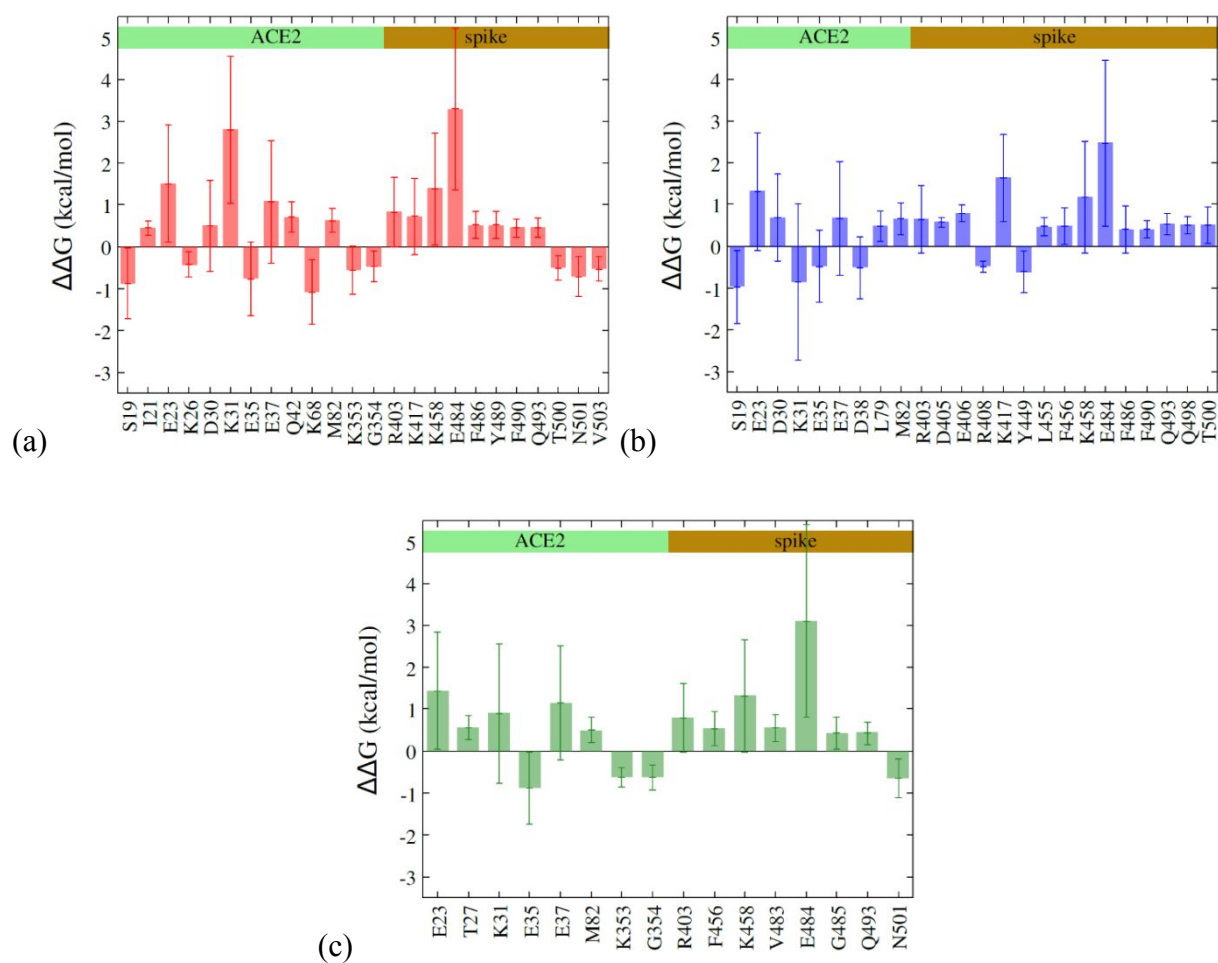


**Figure 6.** Binding free energy change ( $\Delta\Delta G^i$ ) obtained from MMPBSA calculations for the ACE2 – S-RBD complex due to ACE2 adsorption on silane monolayers (a) CH<sub>3</sub> short, (b) mix short, and (c) mix long. For each silane monolayer, all the residues of the complex, with  $|\Delta\Delta G| \geq 0.4$  kcal/mol, are shown. The standard error is indicated.

1  
2  
3 Our error bars reflect the sensitivity of our results to the conformational change variability  
4 observed between the different simulation replicas and to the position variations with simulation  
5 time, due to thermal agitation.  
6  
7  
8

9  
10 Most of the residues presented in Figure 6, *i.e.* the main residues contributing to the  
11 stabilization or to the destabilization of the adsorbed complex, are located at the interface  
12 between ACE2 and S-RBD (Figure 6). In particular, the apolar residue M82 from ACE2 and  
13 the polar or charged residues E484 and Q493 from S-RBD show a stabilizing effect for all  
14 silane monolayers. However, among the all residues presented Figure 6, those identified as  
15 interfacial hot-spot residues by Laurini et al.<sup>38</sup> have too large error bars to show a strong and  
16 clearly stabilizing or destabilizing effect when ACE2 is adsorbed on the studied monolayers,  
17 except K31 that has a clearly stabilizing effect in the case of the CH<sub>3</sub> short monolayer  
18 (Supporting Information, page S7). Furthermore, some polar or charged residues which do not  
19 belong to the interfacial residues identified in Figure 6 show a stabilizing effect, whatever the  
20 studied silane monolayer, such as the residue E23 from ACE2 and the residue K458 from S-  
21 RBD. Also, the contribution of polar and charged residues in the stabilization of the complex  
22 is higher in the case of the CH<sub>3</sub> short monolayer (8.9 kcal/mol) than in the case of the mix short  
23 (7.6 kcal/mol) and mix long (7.5 kcal/mol) monolayers. This result could explain the highest  
24 complex stabilization observed with the CH<sub>3</sub> short monolayer. So, the increase in the binding  
25 free energy, induced by the adsorption of ACE2 on the three studied silane monolayers, can be  
26 largely explained both by the formation of novel hydrogen bonds and by the increase in the  
27 number of electrostatic interactions between particularly mobile residues of ACE2 and of S-  
28 RBD.  
29  
30  
31  
32  
33  
34  
35  
36  
37  
38  
39  
40  
41  
42  
43  
44  
45  
46  
47  
48  
49  
50  
51  
52  
53

54 Finally, we notice that the sum of the stabilizing and destabilizing contributions of the residues  
55 presented in Figure 6 explains most of the global stabilization of the complex (Table 4). Indeed,  
56 in the case of the mix short monolayer, mix long, and CH<sub>3</sub> short monolayers, the 24, 16, and 24  
57  
58  
59  
60

1  
2  
3 residues with  $|\Delta\Delta G| \geq 0.4$  kcal/mol induce a total stabilization of 10.5 kcal/mol out of 11.7  
4  
5 kcal/mol, 8.9 kcal/mol out of 9.9 kcal/mol, and 9.9 kcal/mol out of 15.2 kcal/mol.  
6  
7

8 **SMD simulations.** The increase in the free binding energy between ACE2 and the SARS-CoV-  
9  
10 2 spike protein due to ACE2 adsorption on the studied silane monolayers was further  
11  
12 investigated by SMD simulations. SMD simulations are performed by applying a harmonic  
13  
14 potential to the center-of-mass of S-RBD in the direction normal to the surface. The system  
15  
16 with the CH<sub>3</sub> short monolayer is not suitable for SMD simulations since S-RBD interacts with  
17  
18 the silane molecules. Thus, SMD simulations are only performed on the ACE2 – S-RBD  
19  
20 the silane molecules. Thus, SMD simulations are only performed on the ACE2 – S-RBD  
21  
22 complex in water without surface and on the complex adsorbed on the mix short and mix long  
23  
24 silane monolayers.  
25  
26

27  
28 For each system, SMD simulations are run from two different initial configurations, selected  
29  
30 among the final states of the simulation replicas modelling the complex in water and the  
31  
32 complex adsorbed on the mix short and mix long monolayers. In this way, the effect of the  
33  
34 variability in the final orientation of the adsorbed complex (highlighted through the different  
35  
36 simulation replicas for each silane monolayer) are taken into account. For each initial  
37  
38 configuration, 20 SMD simulation replicas are performed with a pulling velocity  $v = 2$  m.s<sup>-1</sup>  
39  
40 and a force constant  $k = 100$  pN/nm. Force time curves are shown in Figure 7, while the mean  
41  
42 rupture force values are summarized in Supporting information, Table S3 and histograms of the  
43  
44 rupture forces are given in Supporting information, Figure S5.  
45  
46  
47  
48  
49  
50  
51  
52  
53  
54  
55  
56  
57  
58  
59  
60

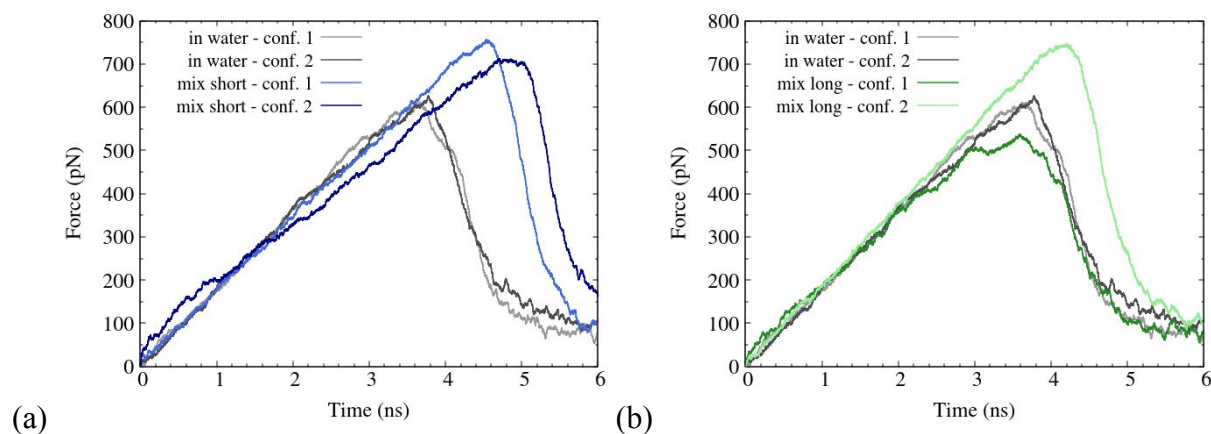


**Figure 7.** Typical force-time curves determined by SMD simulations for the ACE2 – S-RBD complex in water without surface and for ACE2 adsorbed on (a) mix short and (b) mix long silane monolayers.

Regarding the ACE2 – S-RBD complex in water without surface and when the complex is adsorbed on the mix short monolayer, the mean rupture forces from the two initial configurations are close, while with the mix long silane monolayer, we observe different rupture forces for the two initial configurations. These results are in line with the error bars observed in the binding free energy calculations and may be explained by the variability in the adsorption-induced conformational changes for each system. The higher variability obtained with the mix long monolayer could be explained by the lower interactions between ACE2 and S-RBD. However, in line with the binding free energy calculations a clear effect of silane monolayers seems to appear. Indeed, adsorption on the mix short monolayer would lead to a rupture force higher (758 pN and 715 pN for initial configurations 1 and 2) than in water without surface (607 pN and 623 pN for initial configurations 1 and 2). Regarding the mix long monolayer, the rupture force obtained with one of the initial configurations is higher than the values obtained for the complex in water (743 pN), while the value obtained with the other configuration is slightly lower (537 pN). However, results from MMPBSA analysis, which

1  
2  
3 consider the six simulation replicas, would indicate a global increase in the binding free energy  
4 between ACE2 and S-RBD when ACE2 is adsorbed on the mix long silane monolayer. So, as  
5 shown both from MMPBSA calculations and SMD simulations, the studied silane monolayers  
6 would tend to increase by 20% the affinity between ACE2 and S-RBD through the formation  
7 of novel hydrogen bonds and electrostatic interactions at the interface between ACE2 and S-  
8 RBD.  
9

## 18 **Conclusions**

20 The adsorption of ACE2 on six different silane monolayers was studied by MD simulations.  
21 Among them, it was demonstrated that three silane monolayers, CH<sub>3</sub> short, mix short and mix  
22 long would allow to adsorb ACE2 with an orientation compatible with S-RBD trapping. Indeed,  
23 from considerations on the Van der Waals and electrostatic interaction energies, S-RBD binding  
24 pocket on ACE2 should be more likely exposed to the bulk water, in the case of ACE2  
25 adsorption on the mix short and mix long monolayers. In the case of ACE2 adsorption on the  
26 CH<sub>3</sub> short monolayer, S-RBD binding pocket on ACE2 should be close to the silane molecules  
27 but still accessible. RMSD and RMSF, which give information on the global and per residues  
28 conformational changes, appeared similar for ACE2 in water without surface and for ACE2  
29 adsorbed on the studied silane monolayers. So, adsorption on the silane monolayers should not  
30 impact the ability of ACE2 to trap S-RBD. The adsorption of the ACE2 – S-RBD complex  
31 leads to slight conformational changes in residues around the interface between ACE2 and S-  
32 RBD. Our results suggest that these adsorption-induced conformational changes lead to the  
33 formation of novel hydrogen bonds and electrostatic interactions which increase the native  
34 affinity between ACE2 and S-RBD. Interactions are further increased with the CH<sub>3</sub> short  
35 monolayer, than with the mix short monolayer and, than with the mix long monolayer. These  
36 results are in line with the binding free energy calculated by MMPBSA and the rupture forces  
37 calculated by SMD simulations between ACE2 and S-RBD. Consequently, from considerations  
38  
39  
40  
41  
42  
43  
44  
45  
46  
47  
48  
49  
50  
51  
52  
53  
54  
55  
56  
57  
58  
59  
60

1  
2  
3 on the binding free energy but also on the most likely orientation of adsorbed ACE2, the mix  
4 short monolayer might be well-suited to adsorb ACE2, while increasing by 20% its native  
5 affinity towards the SARS-CoV-2 spike protein for biosensing applications. The mix long  
6  
7  
8  
9  
10 monolayer could also be suitable, despite more variability in the results likely because of the  
11  
12 smaller increase in the binding free energy. Such a 20% increase in the binding free energy  
13  
14 could help to improve the efficiency of the current tools using ACE2 for S-RBD detection.<sup>5</sup>  
15  
16 Also, this study suggests that by combining ACE2 adsorption on specific silane monolayers  
17  
18 and the use of ACE2 variants,<sup>6</sup> biosensing tools with efficiency that competes with antigenic  
19  
20 tests, and towards any variants of the SARS-CoV-2 spike protein, could be developed. In order  
21  
22 to sustain our MD results on the adsorption of ACE2 on silane monolayers, experimental  
23  
24 evidences would be needed. Although, the *in-situ* investigations of proteins at solid/liquid  
25  
26 interface remain challenging, a combination of different techniques could help to gain  
27  
28 experimental insights. Among them one can envisioned to study the structure of immobilized  
29  
30 ACE2 by AFM in the Single Molecule Force Spectroscopy mode,<sup>3</sup> by Sum Frequency  
31  
32 Generation vibrational spectroscopy,<sup>40,41</sup> and to measure the affinity between ACE2 and  
33  
34 monoclonal antibodies or/and SARS-CoV-2 spike protein RBD using Surface Plasmon  
35  
36 Resonance. On a longer time scale perspectives, the experimental validation of MD simulations  
37  
38 could help us to select a-priori specific surface modification for protein immobilisation and then  
39  
40 fasten the development of biosensor interfaces.  
41  
42  
43  
44  
45

#### 46 47 SUPPORTING INFORMATION

48  
49 The following files are available free of charge.

50  
51  
52  
53  
54 Total VdW and elec interaction energy between the different silane monolayers and ACE2  
55  
56 cellular receptor. RMSD of ACE2 cellular receptor. RMSF traces of ACE2 cellular receptor.  
57  
58  
59  
60

1  
2  
3 Secondary structure of the ACE2 – S-RBD complex. MMPBSA analysis. Unbinding time and  
4  
5 rupture force from SMD simulations. Rupture force distribution from SMD simulations. (PDF)  
6  
7

## 8 AUTHOR INFORMATION

### 10 **Corresponding Author**

11  
12  
13  
14 \*Email: christelle.yeromonahos@ec-lyon.fr

### 15 **Author Contributions**

16  
17  
18 The manuscript was written through contributions of all authors. All authors have given  
19  
20 approval to the final version of the manuscript.  
21  
22  
23  
24

## 25 ACKNOWLEDGMENT

26  
27  
28 The authors thank Laurent Pouilloux, Anne Cadiou, and Laurent Carrel for support on PMCS2I  
29  
30 resources. S. L. is grateful to the “doctoral school Material” from the University of Lyon,  
31  
32 France, for offering a Ph.D. fellowship.  
33  
34  
35

### 36 **Funding Sources**

37  
38  
39 This work was supported by the Young Researcher ANR PORIDG project, grant ANR-18-  
40  
41 CE09-0006 of the French Agence Nationale de la Recherche. This work was granted access to  
42  
43 the HPC resources of CINES under the allocation 2019-A0070711100 made by GENCI. Also,  
44  
45 this work was supported by the PMCS2I - supercomputer Newton from Ecole Centrale de Lyon,  
46  
47 France, member of the FLMSN.  
48  
49  
50

## 51 REFERENCES

52  
53  
54 (1) Holmes, K. V. Coronaviruses (Coronaviridae) *Encyclopedia of Virology* **1999**, 291–298.  
55  
56  
57  
58  
59  
60

- 1  
2  
3 (2) Wrapp, D.; Wang, N.; Corbett, K. S.; Goldsmith, J. A.; Hsieh, C.-L.; Abiona, O.; Graham,  
4 B. S.; McLellan, J. S. Cryo-EM Structure of the 2019-NCoV Spike in the Prefusion  
5 Conformation. *Science* **2020**, *367*, 1260–1263.  
6  
7  
8  
9  
10 (3) Yang, J.; Petitjean, S. J. L.; Koehler, M.; Zhang, Q.; Dumitru, A. C.; Chen, W.; Derclaye,  
11 S.; Vincent, S. P.; Soumillion, P.; Alsteens, D. Molecular interaction and inhibition of SARS-  
12 CoV-2 binding to the ACE2 receptor. *Nature Communications* **2020**, *11*, 4541.  
13  
14  
15  
16  
17 (4) Li, F. Structure, function, and evolution of coronavirus spike proteins. *Annual review of*  
18 *virology* **2016**, *3*, 237–261.  
19  
20  
21  
22 (5) Al Ahmad, M.; Mustafa, F.; Panicker, N.; Rizvi, T. A. Development of an Optical Assay to  
23 Detect SARS-CoV-2 Spike Protein Binding Interactions with ACE2 and Disruption of these  
24 Interactions Using Electric Current. **2020**, *medRxiv*.  
25  
26  
27  
28  
29 (6) Chan, K. K.; Dorosky, D.; Sharma, P.; Abbasi, S. A.; Dye, J. M.; Kranz, D. M.; Herbert, A.  
30 S.; Procko, E. Engineering human ACE2 to optimize binding to the spike protein of SARS  
31 coronavirus 2. *Science* **2020**, *369*, 1261–1265.  
32  
33  
34  
35  
36 (7) Piplani, S.; Singh, P. K.; Winkler, D. A.; Petrovsky, N. In silico comparison of spike protein-  
37 ACE2 binding affinities across species; significance for the possible origin of the SARS-CoV-  
38 2 virus. **2020**, *arXiv preprint arXiv:2005.06199*.  
39  
40  
41  
42 (8) Chen, Y.; Guo, Y.; Pan, Y.; Zhao, Z. J. Structure Analysis of the Receptor Binding of 2019-  
43 nCoV. *Biochem. Biophys. Res. Commun.* **2020**, *525*, 135–140.  
44  
45  
46  
47 (9) Yan, R.; Zhang, Y.; Li, Y.; Xia, L.; Guo, Y.; Zhou, Q. Structural Basis for the Recognition  
48 of SARS-CoV-2 by Full-Length Human ACE2. *Science* **2020**, *367*, 1444–1448.  
49  
50  
51  
52 (10) He, J.; Tao, H.; Yan, Y.; Huang, S.-Y.; Xiao, Y. Molecular Mechanism of Evolution and  
53 Human Infection with SARS-CoV-2. *Viruses* **2020**, *12*, 428.  
54  
55  
56  
57  
58  
59  
60

- 1  
2  
3 (11) Sumbul, F.; Valotteau, C.; Fernandez, I.; Meola, A.; Baquero, E.; Kostrz, D.; Gosse, C.;  
4 Strick, T. R.; Rey, F.; Rico, F. Dynamics and Binding Strength of the Spike Protein of Sars-  
5 Cov-2 Probed by High-Speed Atomic Force Microscopy. *Biophys. J.* **2021**, *120*, 3a.  
6  
7  
8  
9  
10 (12) Hanson, Q. M.; Wilson, K. M.; Shen, M.; Itkin, Z.; Eastman, R. T.; Shinn, P.; Hall, M. D.  
11 Targeting ACE2–RBD Interaction as a Platform for COVID-19 Therapeutics: Development  
12 and Drug-Repurposing Screen of an AlphaLISA Proximity Assay. *ACS Pharmacol. Transl. Sci.*  
13 **2020**, *3*, 1352–1360.  
14  
15  
16  
17  
18 (13) Basu, A.; Sarkar, A.; Maulik, U. Molecular Docking Study of Potential Phytochemicals  
19 and Their Effects on the Complex of SARS-CoV2 Spike Protein and Human ACE2. *Scientific*  
20 *Reports* **2020**, *10*, 17699.  
21  
22  
23  
24  
25 (14) Bernardi, A.; Huang, Y.; Harris, B.; Xiong, Y.; Nandi, S.; McDonald, K. A.; Faller, R.  
26 Development and Simulation of Fully Glycosylated Molecular Models of ACE2-Fc Fusion  
27 Proteins and Their Interaction with the SARS-CoV-2 Spike Protein Binding Domain. *PLOS*  
28 *ONE* **2020**, *15*, e0237295.  
29  
30  
31  
32 (15) Lan, J.; Ge, J.; Yu, J.; Shan, S.; Zhou, H.; Fan, S.; Zhang, Q.; Shi, X.; Wang, O.; Zhang,  
33 L. et al. Structure of the SARS-CoV-2 spike receptor-binding domain bound to the ACE2  
34 receptor. *Nature* **2020**, *581*, 215–220.  
35  
36  
37  
38 (16) Wang, Q.; Zhang, Y.; Wu, L.; Niu, S.; Song, C.; Zhang, Z.; Lu, G.; Qiao, C.; Hu, Y.;  
39 Yuen, K.-Y.; et al. Structural and Functional Basis of SARS-CoV-2 Entry by Using Human  
40 ACE2. *Cell* **2020**, *181*, 894–904.  
41  
42  
43  
44  
45 (17) Yang, Z.; Chevlot, Y.; Gehin, T.; Dugas, V.; Xanthopoulos, N.; Laporte, V.; Delair, T.;  
46 Ataman-Önal, Y.; Choquet-Kastylevsky, G.; Souteyrand, E.; et al. Characterization of Three  
47 Amino-Functionalized Surfaces and Evaluation of Antibody Immobilization for the Multiplex  
48 Detection of Tumor Markers Involved in Colorectal Cancer. *Langmuir* **2013**, *29*, 1498–1509.  
49  
50  
51  
52  
53  
54  
55  
56  
57  
58  
59  
60

1  
2  
3 (18) Yang, Z.; Chevolut, Y.; Gehin, T.; Solassol, J.; Mange, A.; Souteyrand, E.; Laurenceau,  
4 E. Improvement of Protein Immobilization for the Elaboration of Tumor-Associated Antigen  
5 Microarrays: Application to the Sensitive and Specific Detection of Tumor Markers from Breast  
6 Cancer Sera. *Biosens. Bioelectron.* **2013**, *40*, 385–392.  
7  
8  
9

10  
11  
12 (19) Lecot, S.; Chevolut, Y.; Phaner-Goutorbe, M.; Yeromonahos, C. Impact of Silane  
13 Monolayers on the Adsorption of Streptavidin on Silica and its Subsequent Interactions with  
14 Biotin: Molecular Dynamics and Steered Molecular Dynamics Simulations. *J. Phys. Chem. B*  
15 **2020**, *124*, 6786–6796.  
16  
17  
18  
19

20  
21  
22 (20) Rico, F.; Russek, A.; González, L.; Grubmüller, H.; Scheuring, S. Heterogeneous and Rate-  
23 Dependent Streptavidin–Biotin Unbinding Revealed by High-Speed Force Spectroscopy and  
24 Atomistic Simulations. *Proc. Natl. Acad. Sci. U.S.A.* **2019**, *116*, 6594–6601.  
25  
26  
27  
28

29  
30 (21) Roscioni, O. M.; Muccioli, L.; Mityashin, A.; Cornil, J.; Zannoni, C. Structural  
31 Characterization of Alkylsilane and Fluoroalkylsilane Self-Assembled Monolayers on SiO<sub>2</sub> by  
32 Molecular Dynamics Simulations. *J. Phys. Chem. C* **2016**, *120*, 14652–14662.  
33  
34  
35  
36

37  
38 (22) Lecot, S.; Lavigne, A.; Yang, Z.; Chevolut, Y.; Phaner-Goutorbe, M.; Yeromonahos, C.  
39 Effects of the Chemical and Structural Properties of Silane Monolayers on the Organization of  
40 Water Molecules and Ions at Interfaces, from Molecular Dynamics Simulations. *Langmuir*  
41 **2021**, *37*, 5563–5572.  
42  
43  
44  
45

46  
47 (23) Lecot, S.; Lavigne, A.; Yang, Z.; Géhin, T.; Botella, C.; Jousseau, V.; Chevolut, Y.;  
48 Phaner-Goutorbe, M.; Yeromonahos, C. Arrangement of Monofunctional Silane Molecules on  
49 Silica Surfaces: Influence of the Alkyl Chain Length, Head-Group Charge and Surface  
50 Coverage, from Molecular Dynamics Simulations, X-Ray Photoelectron Spectroscopy and  
51 Fourier Transform Infrared Spectroscopy Analysis. *J. Phys. Chem. C* **2020**, *124*, 20125–20134.  
52  
53  
54  
55  
56  
57  
58  
59  
60

- 1  
2  
3 (24) Van Der Spoel, D.; Lindahl, E.; Hess, B., Groenhof, G.; Mark, A. E.; Berendsen, H. J.  
4 GROMACS: Fast, Flexible, and Free. *J. Comput. Chem.* **2005**, *26*, 1701–1718.  
5  
6  
7  
8 (25) Humphrey, W.; Dalke, A.; Schulten, K. VMD: Visual Molecular Dynamics. *J. Mol. Graph.*  
9 **1996**, *14*, 33–38.  
10  
11  
12  
13 (26) Jorgensen, W. L.; Maxwell, D. S.; Tirado-Rives, J. Development and Testing of the OPLS  
14 All-Atom Force Field on Conformational Energetics and Properties of Organic Liquids. *J. Am.*  
15 *Chem. Soc.* **1996**, *118*, 11225–11236.  
16  
17  
18  
19 (27) Castillo, J. M.; Klos, M.; Jacobs, K.; Horsch, M.; Hasse, H. (2015). Characterization of  
20 Alkylsilane Self-Assembled Monolayers by Molecular Simulation. *Langmuir* **2015**, *31*, 2630–  
21 2638.  
22  
23  
24  
25  
26  
27  
28 (28) Jorgensen, W. L.; Gao, J. Monte Carlo Simulations of the Hydration of Ammonium and  
29 Carboxylate Ions. *J. Phys. Chem.* **1986**, *90*, 2174–2182.  
30  
31  
32  
33 (29) Jorgensen, W. L., Chandrasekhar, J.; Madura, J. D. Comparison of Simple Potential  
34 Functions for Simulating Liquid Water. *J. Chem. Phys.* **1983**, *79*, 926–935.  
35  
36  
37  
38 (30) Aqvist, J. Ion-Water Interaction Potentials Derived from Free Energy Perturbation  
39 Simulations. *J. Phys. Chem.* **1990**, *94*, 8021–8024.  
40  
41  
42  
43 (31) Chandrasekhar, J.; Spellmeyer, D. C.; Jorgensen, W.L. Energy Component Analysis for  
44 Dilute Aqueous Solutions of Lithium (1+), Sodium (1+), Fluoride (1-), and Chloride (1-) Ions.  
45 *J. Am. Chem. Soc.* **1984**, *106*, 903–910.  
46  
47  
48  
49 (32) Kitabata, M.; Taddese, T.; Okazaki, S. Molecular Dynamics Study on Wettability of Poly  
50 (vinylidene fluoride) Crystalline and Amorphous Surfaces. *Langmuir* **2018**, *34*, 12214–12223.  
51  
52  
53  
54 (33) Kumari, R.; Kumar, R.; Lynn, A. g\_mmpbsa – A GROMACS Tool for High-Throughput  
55 MM-PBSA Calculations. *J. Chem. Inf. Model.* **2014**, *54*, 1951–1962.  
56  
57  
58  
59  
60

1  
2  
3 (34) Ali, A.; Vijayan, R. Dynamics of the ACE2–SARS-CoV-2/SARS-CoV spike protein  
4 interface reveal unique mechanisms. *Sci. Rep.* **2020**, *10*, 14214.  
5  
6

7  
8 (35) Quan, X.; Liu, J.; Zhou, J. Multiscale modeling and simulations of protein adsorption:  
9 progresses and perspectives. *Curr. Opin. Colloid Interface Sci.* **2019**, *41*, 74–85.  
10  
11

12  
13 (36) Zhou, J.; Zheng, J.; Jiang, S. Molecular simulation studies of the orientation and  
14 conformation of cytochrome c adsorbed on self-assembled monolayers. *J Phys Chem B* **2004**,  
15 *108*, 17418–17424.  
16  
17  
18

19  
20 (37) Jurrus, E.; Engel, D.; Star, K.; Monson, K.; Brandi, J.; Felberg, L.E.; Brookes, D.H.;  
21 Wilson, L.; Chen, J.; Liles, K. et al. Improvements to the APBS biomolecular solvation software  
22 suite. *Protein Sci.* **2018**, *27*, 112–128.  
23  
24  
25  
26

27  
28 (38) Laurini, E.; Marson, D.; Aulic, S.; Fermeglia, M.; Pricl, S. Computational Alanine  
29 Scanning and Structural Analysis of the SARS-CoV-2 Spike Protein/Angiotensin-Converting  
30 Enzyme 2 Complex. *ACS Nano* **2020**, *14*, 11821–11830.  
31  
32  
33

34  
35 (39) Laurini, E.; Marson, D.; Aulic, S.; Fermeglia, A.; Pricl, S. Computational Mutagenesis at  
36 the SARS-CoV-2 Spike Protein/Angiotensin-Converting Enzyme 2 Binding Interface:  
37 Comparison with Experimental Evidence. *ACS Nano* **2021**, *15*, 6929–6948.  
38  
39  
40  
41

42  
43 (40) Guo, W.; Zou, X.; Jiang, H.; Koebeke, K.J.; Hoarau, M.; Crisci, R.; Lu, T.; Wei, T.; Neil,  
44 E.; Marsh, G. et al. Molecular Structure of the Surface-Immobilized Super Uranyl Binding.  
45 *Protein J. Phys. Chem. B* **2021**, *125*, 7706–7716.  
46  
47  
48  
49

50  
51 (41) Hosseinpour, S.; Roeters, S. J.; Bonn, M.; Peukert, W.; Woutersen, S.; Weidner, T.  
52 Structure and Dynamics of Interfacial Peptides and Proteins from Vibrational Sum-Frequency  
53 Generation Spectroscopy. *Chem. Rev.* **2020**, *120*, 3420–3465.  
54  
55  
56  
57

58  
59 **TOC graphic**  
60

